CSIRO PUBLISHING

www.publish.csiro.au/journals/mfr *Marine and Freshwater Research*, 2005, **56**, 795–804

Otolith shape contour analysis using affine transformation invariant wavelet transforms and curvature scale space representation

V. Parisi-Baradad[A,D], *A. Lombarte*[B], *E. Garcia-Ladona*[B], *J. Cabestany*[A], *J. Piera*[C] *and O. Chic*[B]

[A]Departament d'Enginyeria Electrònica, Universitat Politècnica de Catalunya, c./ Jordi Girona 31, Barcelona 08034, Catalunya, Spain.
[B]Institut de Ciències del Mar (CMIMA-CSIC), Passeig Marítim 37-49, Barcelona 08003, Catalunya, Spain.
[C]Departament de Teoria del Senyal i Comunicacions, Universitat Politècnica de Catalunya, Avgda. Canal Olimpic s/n, Castelldefels 08860, Catalunya, Spain.
[D]Corresponding author. Email: parisi@eel.upc.es

Abstract. Fish otolith morphology has been closely related to landmark selection in order to establish the most discriminating points that can help to differentiate or find common characteristics in sets of otolith images. Fourier analysis has traditionally been used to represent otolith images, since it can reconstruct a version of the contour that is close to the original by choosing a reduced set of harmonic terms. However, it is difficult to locate the contour's singularities from this spectrum. As an alternative, wavelet transform and curvature scale space representation allow us to quantify the irregularities of the contour and determine its precise position. These properties make these techniques suitable for pattern recognition purposes, ageing, stock determination and species identification studies. In the present study both techniques are applied and used in an otolith classification system that shows robustness against affine image transformations, shears and the presence of noise. The results are interpreted and discussed in relation to traditional morphology studies.

Extra keywords: curvature scale space, fish otolith, Fourier harmonic, shape analysis, wavelet transform.

Introduction

Fish stocks, populations and species can be inferred from the size and shape of their otoliths (Yefanov and Khorevin 1979; Nolf 1985; Messieh *et al*. 1989; Castonguay *et al*. 1991; Campana and Casselman 1993; Friedland and Reddin 1994; Torres *et al*. 2000; Cardinale *et al*. 2004). Since the 1990s, these tasks have been performed by determining morphological features of the whole otolith outline contour based on the one-dimensional representation of its perimeter. This curve is obtained by decomposing the contour into several fragments and calculating the distances between the end of each fragment and the centre of gravity of the analysed otolith. The main problem then is how to discriminate between the one-dimensional representations of otolith contours of different species, populations, stocks, etc. A popular and commonly used method for doing this is to apply an harmonic expansion using a Fourier transform (FT) (Bird *et al*. 1986; Castonguay *et al*. 1991; Campana and Casselman 1993). This consists of a representation decomposing the curve into a linear combination of sinus and cosinus functions that allow us to obtain the spectrum representation of the otolith contour which can serve to characterise the otolith shape. Low wave numbers determine the overall otolith shape while high wave numbers represent smaller irregularities (Zahn and Roskies 1972). Working with this type of representation allows us to implement a pattern recognition and classification system based, for example, on the mean square distances in Fourier space easily. Roughly speaking otoliths with a similar spectrum, or analogous Fourier decomposition, should share similar shape characteristics.

However, Fourier decomposition is defined by an integral expression over the whole closed curve and its capability to locate and discriminate different singularities, which may appear very close together and with different sizes, is questionable. In addition signal analysis theory has shown that localised sharp irregularities within a signal are not well captured by Fourier analysis because they expand into a large number of high order harmonics, which makes it difficult to provide a clear representation of morphological features. Alternatively, relatively recent signal processing techniques, such as wavelet transform (WT) and curvature scale space (CSS) representation, solve these problems much more efficiently and adequately. Intuitively, both are more related to landmark selection usually carried out by trained human

 10.1071/MF04162 1323-1650/05/050795

operators who manually obtain morphological features for classification. Mathematically speaking, WT is a way to expand a signal into a family of functions that represent the dilations and translations of a unique function known as a mother wavelet, located both in space and wave number. The WT has the ability not only to measure sharp transitions of the signal but also to establish its location (Mallat 1989). However, the CSS representation (Mokhtarian and Mackworth 1992) is a technique that focuses on finding the curvature changes of a contour, called the inflection points, and analyses how they change after successive smoothing of the curve. The curve description in this technique does not vary in relation to scale transformations, translations and rotations of the image.

Thus, the main purpose of the current article is to show the advantages of using both techniques to characterise the shape of otoliths better. In the following section we describe in detail how these techniques are applied to analyse and extract the mathematical information that characterises otolith contours. In addition we present some results to test the robustness and the ability of these representations to be used as a pattern recognition technique for discriminating otolith shapes. Finally we discuss and compare the performance of each technique.

Table 1. Nothotenid species from the database analysed, number of specimens and total length range of each database species

Species	No. specimens	Total length range (cm)
Aethotaxis mitopteryx	8	30–49
Dissostichus mawsoni	7	36–38
Gobionotothen gibberifrons	7	35–44
Lepidonotothen larseni	10	14–19
Lepidonotothen nudifrons	13	8–18
Pleuragramma antarcticum	8	13–23
Trematomus bernacchii	8	19–34
Trematomus eulepidotus	13	13–31
Trematomus hansoni	13	24–40
Trematomus lepidorhinus	12	12–27
Trematomus loennbergii	7	26–32
Trematomus nicolai	10	20–34
Trematomus pennellii	13	7–25
Trematomus scotti	13	6–16

Materials and methods

Throughout the present paper we use examples of contours extracted from otolith images belonging to a collection available at the Institut de Ciències del Mar de Barcelona (CSIC) and associated with the AFORO database (http://www.cmima.csic.es/aforo/, verified June 2005). At present, the AFORO database includes around 900 high-resolution images corresponding to 182 species and 71 families mainly from the Western Mediterranean, the Weddell Sea and Antartic Peninsula. From this database we selected a subset of otoliths from the *Nototheniidae* family (Table 1). This is the largest group of the Antarctic ichthyiofauna, characterised by high morphological diversity, which is also manifested in the otolith shape as a consequence of the radiative evolution process (Klingenberg and Ekau 1996; Eastman and Clarke 1998). The images are all coded in eight-bit depth grey scale and captured at different pixel resolutions in order to record the most important details (Fig. 1).

Before making the shape analysis, otolith border detection is a crucial step for obtaining the highest quality data information. Object edges are usually detected through gradient-based techniques that measure the

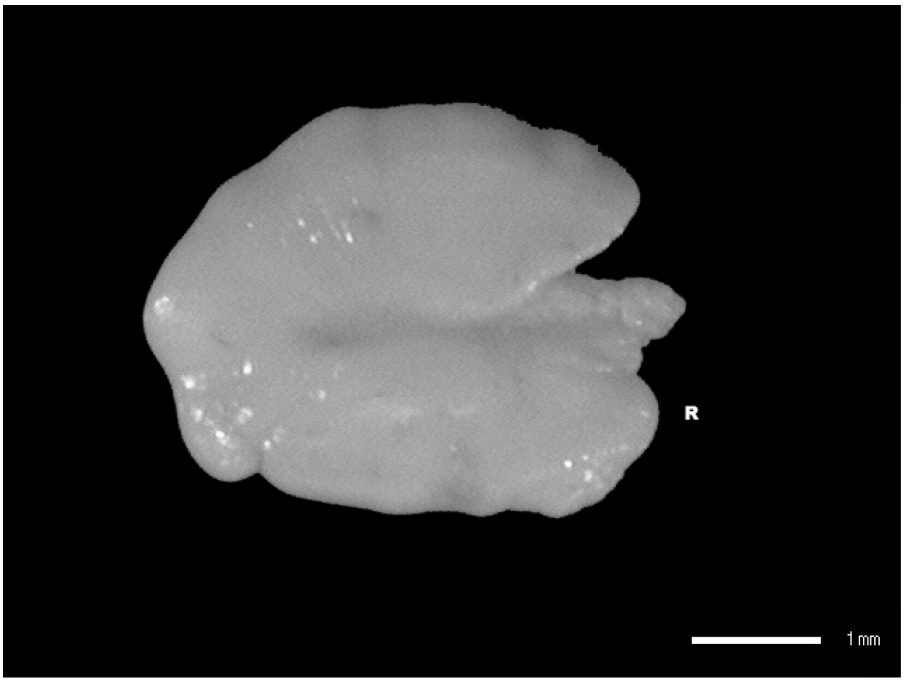

Fig. 1. Image of the left otolith sagita from a *Dissostichus mawsoni* specimen.

directional derivatives of the image components. Even though there are approaches based on differential operators that are very robust to noise and can compute a precise edge location (Marr and Hildreth 1980; Canny 1986), we decided to use the Sobel detector (Nixon and Aguado 2002), which in our case, correctly solved the image edges as well as being simple to use. This detector is based on a convolution of the image to be processed with the horizontal (h) and vertical (v) derivative masks computed through the following matrix operators:

$$h = \begin{bmatrix} -1 & 0 & 1 \\ -2 & 0 & 2 \\ -1 & 0 & 1 \end{bmatrix} \qquad v = \begin{bmatrix} -1 & -2 & -1 \\ 0 & 0 & 0 \\ 1 & 2 & 1 \end{bmatrix} \tag{1}$$

Even though the images are usually acquired under rather good laboratory conditions, they cannot be totally controlled and the sample image to be recognised can differ in pixel resolution, orientation, position and camera alignment with respect to the reference images. Under such conditions it is difficult to set a gradient threshold to determine the otolith contour so that all the points are connected giving a closed curve. To solve this problem, morphological dilation and erosion were applied after thresholding the Sobel filtered image. The dilation operation consists in a gradual thickening of the pixels of a contour in a binary image. That is, all the pixels in an eight neighbourhood of a contour pixel are set to 1, while erosion performs a dual operation: it erases any pixel in a dilated image whose eight neighbours aren't all equal to one. Once the contour thickness is 1 pixel, it can be extracted and parameterised in different ways according to the analysis and representation methods used in this work. We considered the centre of gravity of each contour as the origin of the coordinates. All contours were interpolated with a cubic spline, low pass filtered and resampled to 512 points. This is a compromise to minimise the computational load, by using fast numerical implementations, and at the same time keep the prominent details in each representation (radius *v.* angle in WT and contour coordinates *v.* arc length in CSS).

Curvature scale space

The CSS representation (Mokhtarian and Mackworth 1992) is based on the curvature function of the shape contour. The curvature measures the rate of change in the edge direction, characterising in this way the points along the contour. Points in a straight line with no flexions have zero curvature. A circle has constant curvature and an irregular contour has a curvature that increases with the bending of the irregularities (corners, protuberances).

The CSS finds the borders between interesting segments, by searching for points of zero curvature, this is done at different spatial scales or zoom levels to focus on all the irregular (not straight) structures whatever their size. This spatial selection is achieved by iteratively filtering the contour with a Gaussian-like function. Its support is increased progressively in order to analyse all the contour details, finishing when all the irregularities have been removed and the contour has a smooth shape.

The set of inflection points (CSS) constitutes a shape descriptor that does not change when the contour undergoes displacements or rotations, and can be easily normalised to a fixed contour length, thus it will not be affected by affine image transformations (translation or angular changes of the image axis).

The curvature κ of a contour, represented by its pixel coordinates $\Gamma(u) = (x(u), y(u))$ as a function of the arc length u, is defined as (Courant and John 1989):

$$\kappa(u) = \frac{\dot{x}(u)\ddot{y}(u) - \ddot{x}(u)\dot{y}(u)}{(\dot{x}^2(u) + \dot{y}^2(u))^{3/2}} \tag{2}$$

where the number of dots over a variable indicates the order of derivative.

This expression uses all the details of the contour, and to focus on a spatial scale we can filter the contour with a Gaussian function

$$g(u, \sigma) = \frac{1}{\sqrt{2\sigma^2}} e^{-u^2/2\sigma^2} \tag{3}$$

where σ is the scaling parameter (the smoothness degree). The curvature of the smoothed contour, at a given scale (σ) is then computed by:

$$\kappa(u, \sigma) = \frac{\dot{X}(u, \sigma)\ddot{Y}(u, \sigma) - \ddot{X}(u, \sigma)\dot{Y}(u, \sigma)}{(\dot{X}^2(u, \sigma) + \dot{Y}^2(u, \sigma))^{3/2}} \tag{4}$$

where $X(u, \sigma)$ and $Y(u, \sigma)$ are filtered values.

Figure 2 shows a polar representation of the contour extracted from the otolith image appearing in Fig. 1. We can observe three salient structures that characterise this shape. Its location and shape are unambiguous descriptors of this otolith. Figure 3 is the CSS representation for the otolith shown in Fig. 1. The location of the inflection points is plotted at each scale-angle pair. As we increase the scale (degree of smoothness) the number of inflexion points decreases, in other words, the shape becomes more and more rounded. For this otolith we can see three main elongated patterns that correlate with the structures observed in the polar representation (Fig. 2). This is a common feature of the CSS representation, the set of inflexion points at relevant structures in all the spatial scales gives rise to elongated patterns that progress vertically as the scale increases. The more prominent the irregularity the taller the associated CSS pattern. In addition, the CSS representation easily locates the position of such structures in the system coordinates.

The CSS is therefore a helpful tool to perform morphological studies where structure size and location is an important issue. Moreover, it provides a unique and stable representation of a contour, i.e. small variations in the contour slightly modify the CSS pattern, which is a suitable property for pattern recognition purposes.

Wavelet transform

The WT is another representation where resolution is adapted to the size of the structures. The WT compares the signal to a finite length analysing the function called wavelet in a set of increasing scales that are obtained by dilating the wavelet. The WT ($W_s\rho(\varphi)$) of the otolith radius ρ at scale s, computes the resemblance of the otolith radius to a wavelet function ψ_s, of zero mean and finite length, dilated by a scaling factor:

$$\psi_s(x) = \frac{1}{s}\psi\left(\frac{\varphi}{s}\right) \tag{5}$$

This resemblance is obtained by the convolution product of the signal to the wavelet at each angle φ, defined as:

$$W_s\rho(\varphi) = \rho^*\psi_s(\varphi) = \int_{-\infty}^{+\infty} \rho(\beta)\psi_s(\varphi - \beta)d\beta \tag{6}$$

where * symbolises the convolution product.

Choosing the appropriate wavelet shape and setting a scaling parameter allows the wavelet transform to detect singularities of different sizes in the analysed signal. Usually the scaling factor is reduced to a finite range of dyadic scales ($s = 2^j$, $j \in Z$), where the smallest scale we use is 1 and the largest is 2^J.

Mallat (1989) associates the wavelet with a blurring function ϕ, to obtain the smoothed components of the transformed signal that remain after the wavelet transform is computed at each scale

$$S_{2^j}\rho(\varphi) = \rho^*\phi_{2^j}(\varphi) \tag{7}$$

interprets the wavelet transform at scales from 2^1 to 2^J, $[W_{2^j}\rho(\varphi)]_{1 \le j \le J}$, as the details of $\rho(\varphi)$ that are in $S_1\rho(\varphi)$ are not in $S_{2^J}\rho(\varphi)$.

The successive convolution of the radius with the wavelet and blurring filters produces a complete representation (discrete wavelet

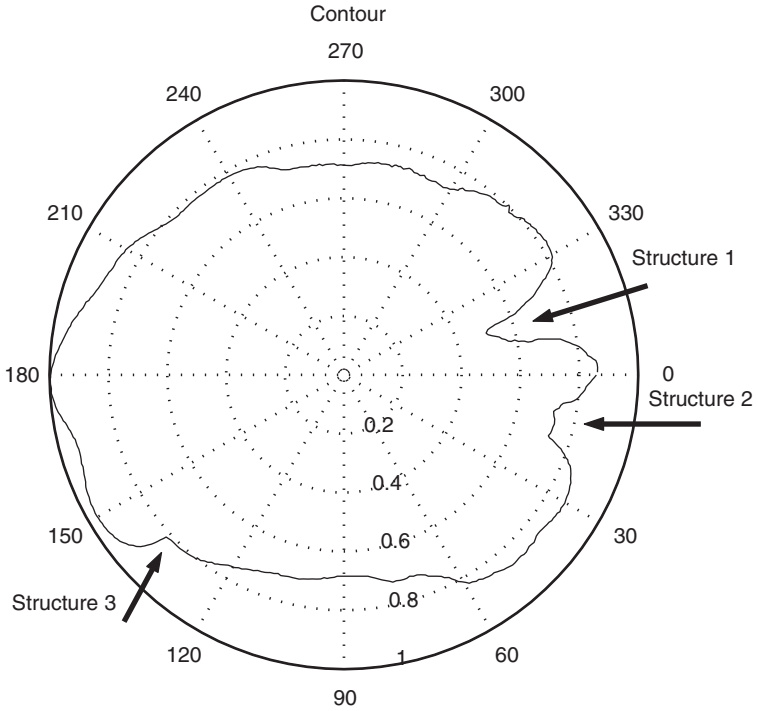

Fig. 2. Planar polar representation of the otolith contour extracted from original image shown in Fig. 1. The contour is resolved by 512 points, sampled in a clockwise sense where the origin is the centroid. 1, 2 and 3 label the three most important structures of the otolith contour.

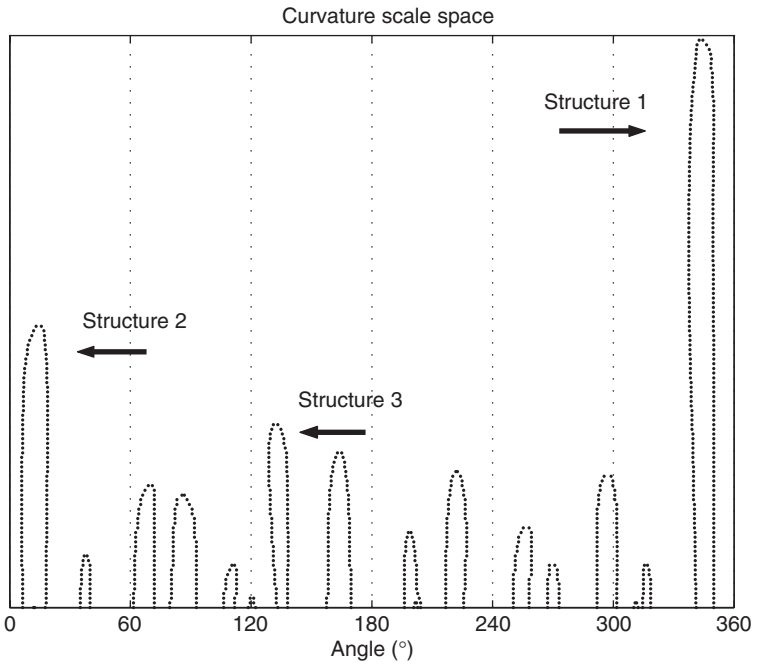

Fig. 3. Curvature scale space (CSS) representation from a *Dissostichus mawsoni* otolith (see Fig. 1). The horizontal axis is the sampling angle and the vertical axis is the scale under analysis in arbitrary units. The three marked structures show the visual cues to identify the otolith shape, that correspond to those marked on Fig. 2.

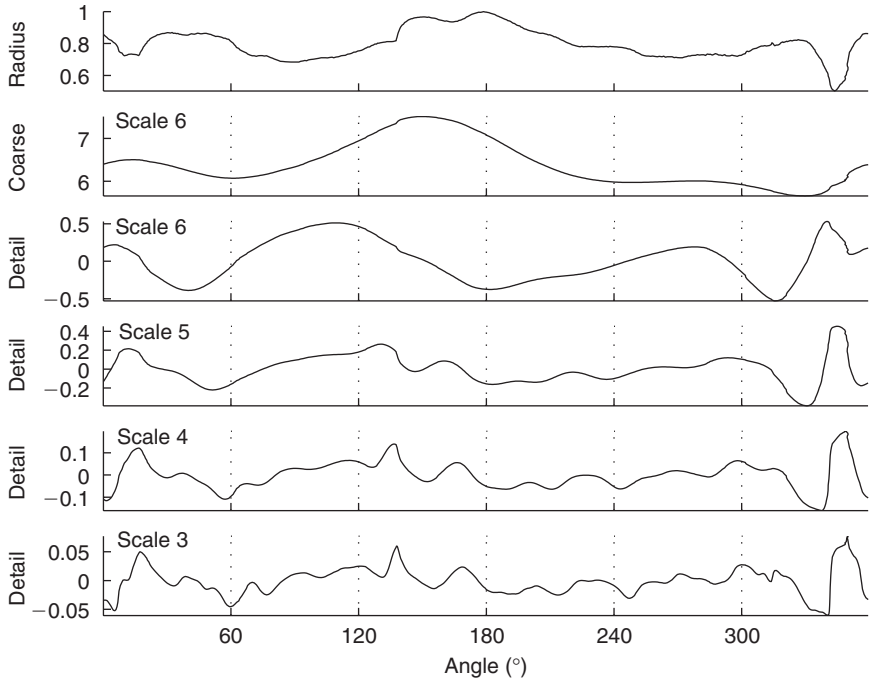

Fig. 4. Wavelet transform (WT) of *Dissostichus mawsoni* otolith (see Fig. 1) computed for scales 3 to 6 (bottom to top). Top image plots the original contour data in cartesian axes. The peaks of the WT at successive scales indicate the main visual cues of the shape. At scale 3 the maxima are located at the contour structures marked in Figs 2 and 3.

transform or DWT), consisting in the details of the radius from scales 2^1 to 2^J plus the remaining, coarse residual signal at scale 2^J:

$$\{S_{2^J}\rho, [W_{2^j}\rho]_{1\le j\le J}\} \tag{8}$$

In this work we use the wavelet mother function, proposed by (Mallat 1991), as the derivative of a quadratic spline function θ:

$$\psi_{2^j}(\varphi) = \frac{d\theta_{2^j}}{d\varphi} \tag{9}$$

$$W_{2^j}\rho(\varphi) = 2^j \frac{d}{d\varphi}(\rho^*\theta_{2^j})(\varphi) \tag{10}$$

Using this wavelet, the fast changing points of an otolith shape appear as large values of the wavelet transform. In Fig. 4 we show an example of the WT computed for a contour of a *Dissostichus mawsoni*. The top signal is the radius ρ plotted against the angle. In the second row we plot the smoothed signal at scale 2^6, and the details from scales 2^6 down to 2^3 are plotted below (for the otoliths belonging to the set used in this work details at scales 2^2 and 2^1 where very small and therefore not used).

When considering the DWT as an analysis tool, it is possible to observe that the points corresponding to the largest structures in the CSS also appear here as peaks of the details at scale 2^1. However, the radius can be seen as a blurred signal given by $S_{2^6}\rho(\varphi)$ plus the details obtained from $W_{2^6}\rho(\varphi)$ to $W_{2^3}\rho(\varphi)$.

Mallat (1991) conjectured that a WT can be closely reconstructed from the positions of its zero crossings $(z_n)_{n\in Z}$ and an integral measure $(e_n)_{n\in Z}$ of the WT between each consecutive pair (z_{n-1}, z_n), computed at all the dyadic scales:

$$e_n = \int_{z_{n-1}}^{z_n} W_{2^j}\rho(\varphi)d\varphi \tag{11}$$

$$Z_{2^j}\rho(\varphi) = \frac{e_n}{z_n - z_{n-1}}, \quad \varphi \in [z_n - z_{n-1}] \tag{12}$$

The sequence $\{Z_{2^j}\rho, 1 \le j \le J\}$ is called the zero crossing representation of ρ. This representation is also very useful in pattern recognition applications since it allows a distance between two different signals f and g to be defined:

$$d(Zf, Zg)^2 = \sum_{j=-\infty}^{\infty} \|Z_{2^j} f(x) - Z_{2^j} g(x)\|^2 \tag{13}$$

which is easy to compute in terms of operations to be carried out, and can be coded in an efficient manner to perform searches in a database of signals based on their most important features.

In Fig. 5 we show the zero crossing representation for the scale 2^6 of the wavelet details shown in Fig. 4.

To compare the analysis performed by WT and the harmonic analysis we have computed the FT of the contour of the *Dissostichus mawsoni* otolith of Fig. 1 and ploted it in Fig. 6. The overall shape of a closed contour FT is mainly represented in low frequency terms and the smaller details appear at faster oscillating harmonics. Thus, even though the FT plot intuitively tells us what its shape is, the structures of the original signal cannot be directly located from the magnitude-phase representation.

Results

Taking into account the properties of the WT and CSS we developed two different applications in order to show their usefulness in fish otolith studies.

The WT, or the Zero Crossings of the WT are idoneus for pattern recognition purposes, therefore we coded a software algorithm to search for an otolith contour in the database. We used the distance Eqn (13) to find the most

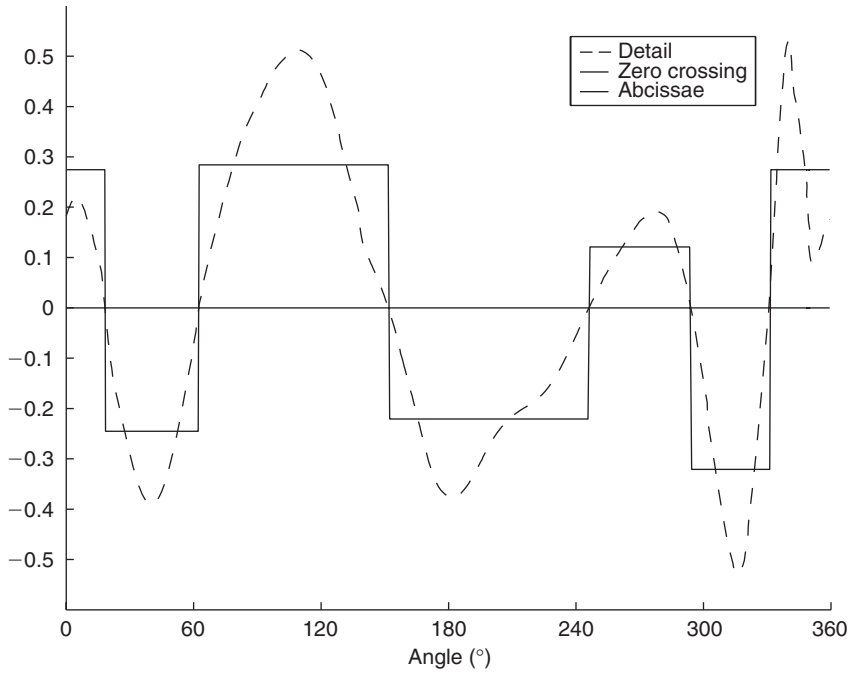

Fig. 5. Zero crossing representation of a *Dissostichus mawsoni* otolith (see Fig. 1) at scale 6. This step like signal, together with the rest of zero crossing signals at all the scales carry all the shape information and is much simpler than the original signal.

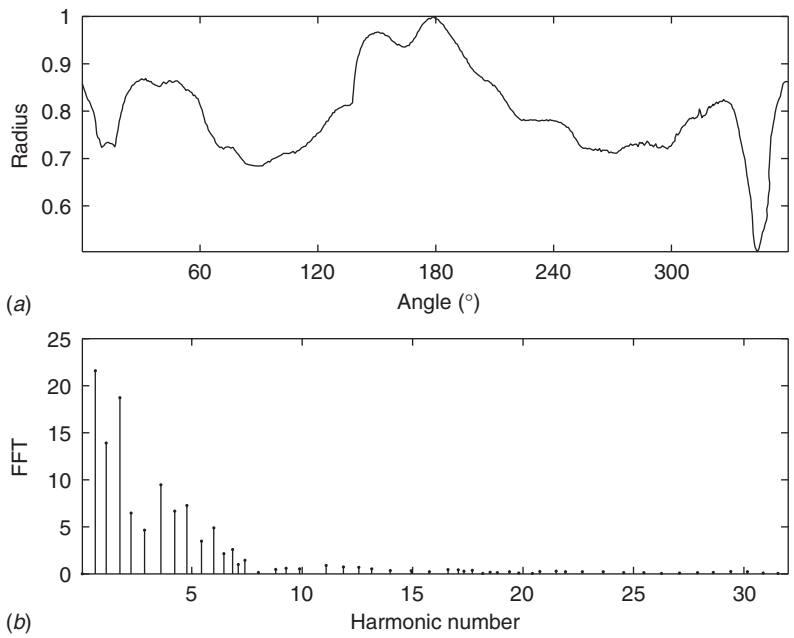

Fig. 6. (*a*) Contour representation of an otolith outline from a *Dissostichus mawsoni* specimen (see Fig. 1). (*b*) Fourier harmonic representation of the same otolith.

similar contours and we searched for five different samples chosen randomly. The samples were from the following species: *Aethotaxis mitopteryx*, *Dissostichus mawsoni*, *Pleuragramma antarcticum*, *Trematomus lepidorhinus* and *Trematomus bernacchii.* Figure 7 shows the output of the algorithm when we searched for an *Aethotaxis mitopteryx*. In the upper most left hand corner we have plotted the searched contour, and the five most similar contours are shown together with a percentage of resemblance. For this search the system found two *Aethotaxis mitopteryx* with very

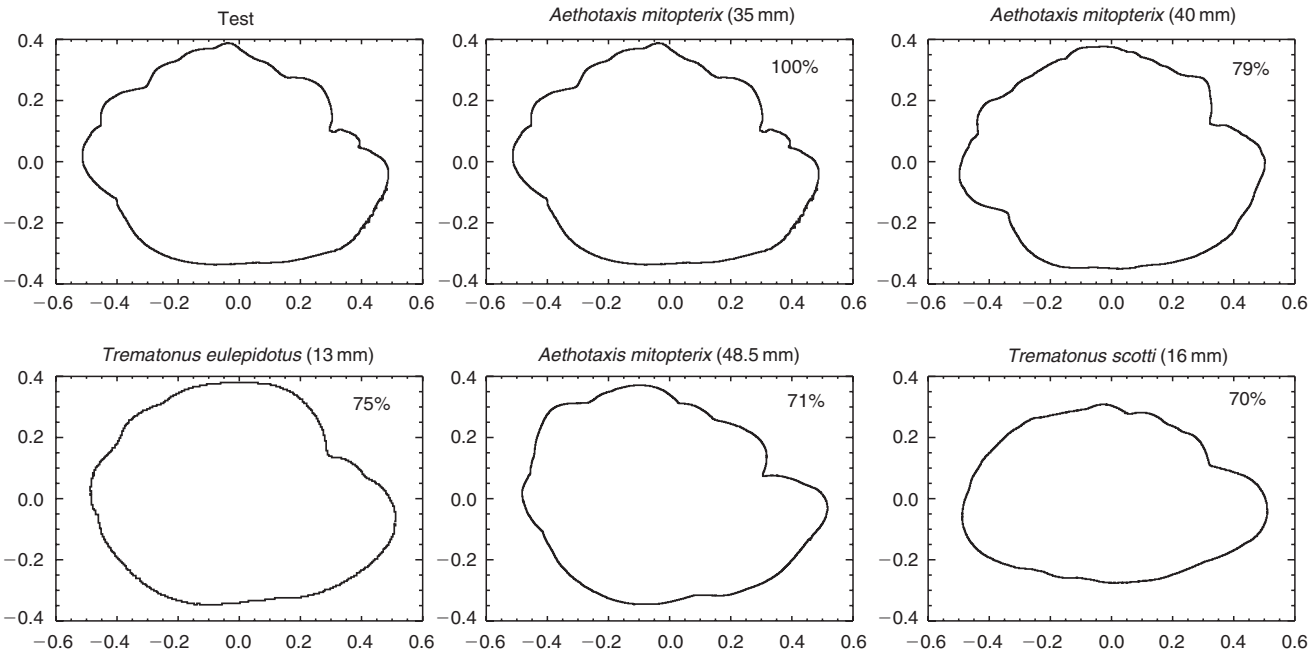

Fig. 7. The five closest otolith obtained when a test otolith (*Aethotaxis mitopteryx*) image is searched for in the database.

Table 2. Results obtained for five different searches in the database

Otolith searched	*Aethotaxis mitopteryx*	*Dissostichus mawsoni*	*Pleuragramma antarcticum*	*Trematomus lepidorhinus*	*Trematomus bernacchii*
1st similar	*Aethotaxis mitopteryx*	*Dissostichus mawsoni*	*Pleuragramma antarcticum*	*Trematomus lepidorhinus*	*Trematomus bernacchii*
2nd similar	*Aethotaxis mitopteryx*	*Dissostichus mawsoni*	*Pleuragramma antarcticum*	*Trematomus lepidorhinus*	*Trematomus bernacchii*
3rd similar	*Trematomus eulepidotus*	*Dissostichus mawsoni*	*Pleuragramma antarcticum*	*Trematomus pennelli*	*Trematomus bernacchii*
4th similar	*Aethotaxis mitopteryx*	*Dissostichus mawsoni*	*Pleuragramma antarcticum*	*Trematomus scotti*	*Trematomus bernacchii*
5th similar	*Aethotaxis mitopteryx*	*Trematomus hansoni*	*Trematomus hansoni*	*Lepidonotothen larseni*	*Trematomus eulepidotus*

similar contours, followed by a *Trematomus eulepidotus* and a *Aethotaxis mitopteryx*. For the rest of the otoliths that we searched for the results appear in Table 2.

The design of an image database retrieval system based on otolith shape has to take into account that the searched images may have affine transformations (scaling, rotation and translation) and also a shear, owing to the transformation of the otolith's intrinsic three-dimensional form into a flat image. To test the performance of the search engine, we artificially provoked a shear with a mathematical transformation of the contour coordinates $\{x(u), y(u)\}$ to obtain the modified contour $\{x^k(u), y^k(u)\}$:

$$\begin{bmatrix} x^k(u) \\ y^k(u) \end{bmatrix} = \begin{bmatrix} 1 & k \\ 0 & 1 \end{bmatrix} \cdot \begin{bmatrix} x^k(u) \\ y^k(u) \end{bmatrix} \qquad (14)$$

Out of all the transformations a shear is the most problematic, since; scaling is solved by normalising the contour length; rotation is manifested as a displacement of the WT and is solved by brute force by computing the distance function (Eqn 14) for different rotation ranges; and translation effects disappear when using the otolith's centre of gravity as the origin of the coordinates. Figure 8 shows a sheared version of the sample of *Trematomus lepidorhinus* used before, and the results obtained. It is possible to see that, even though the sheared otolith loses some of its resemblance to the database original, the search tool still finds two specimens from the same group. A similar performance was obtained for the rest of the otoliths tested, except for *Trematomus lepidorhinus*, which when sheared resembles a *Trematomus pennellii*, however, the second most similar contour found belonged to the same genus (Table 3).

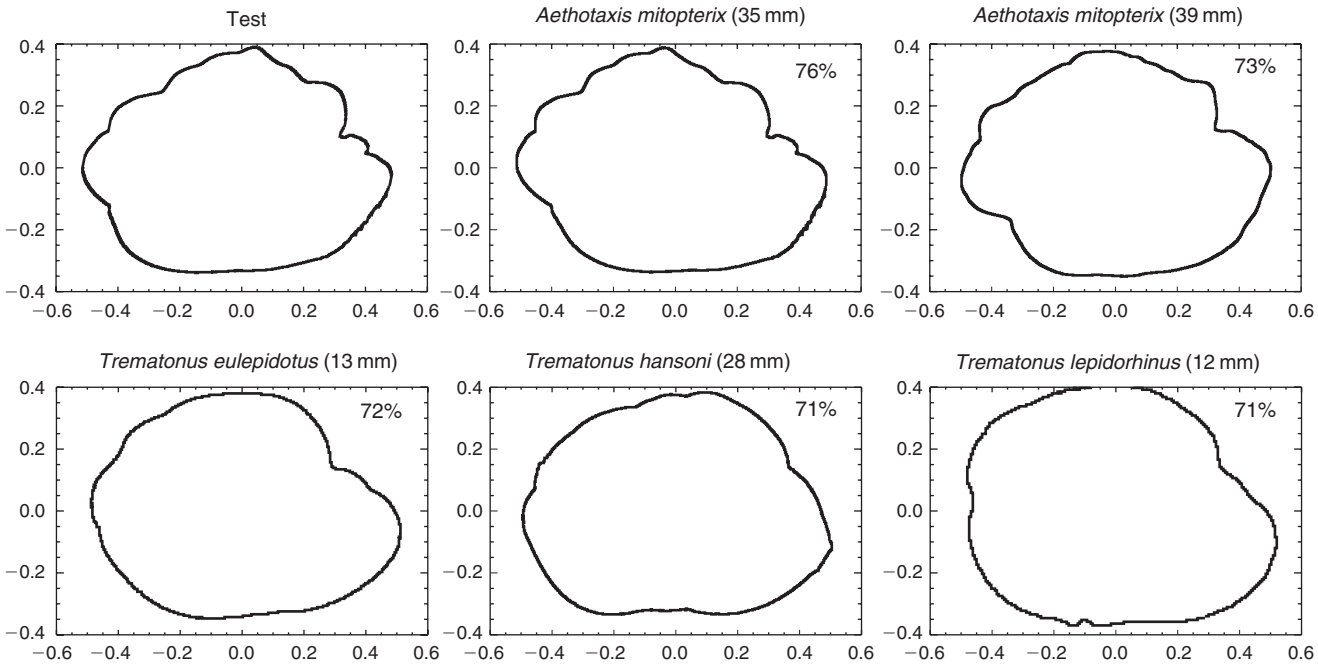

Fig. 8. The five closest otolith obtained when a sheared test otolith (*Aethotaxis mitopteryx*) image is searched for in the database.

Table 3. Results obtained when searching for five different, sheared otoliths in the database

Otolith searched	*Aethotaxis mitopteryx*	*Dissostichus mawsoni*	*Pleuragramma antarcticum*	*Trematomus lepidorhinus*	*Trematomus bernacchii*
1st similar	*Aethotaxis mitopteryx*	*Dissostichus mawsoni*	*Pleuragramma antarcticum*	*Trematomus pennellii*	*Trematomus bernacchii*
2nd similar	*Aethotaxis mitopteryx*	*Dissostichus mawsoni*	*Pleuragramma antarcticum*	*Trematomus lepidorhinus*	*Trematomus bernacchii*
3rd similar	*Trematomus eulepidotus*	*Dissostichus mawsoni*	*Pleuragramma antarcticum*	*Trematomus lepidorhinus*	*Trematomus pennellii*
4th similar	*Trematomus hansoni*	*Dissostichus mawsoni*	*Pleuragramma antarcticum*	*Trematomus lepidorhinus*	*Trematomus pennellii*
5th similar	*Trematomus lepidorhinus*	*Pleuragramma antarcticum*	*Trematomus hansoni*	*Trematomus eulepidotus*	*Trematomus pennellii*

When intraspecies variability was studied, the CSS revealed differences between samples of different sizes. In the case of *Trematomus lepidorhinus*, the smallest specimens basically contain two inflexion points at all the scales, which is related with the escisura ostii (Nolf 1985). When the otolith grows, a change in shape is observed and CSS representation shows an increase in the number of inflexion points indicating a loss of roundness and a progressive elongation and irregularity of the otolith's outline in comparison with smaller ones (Fig. 9).

Discussion

We have introduced two signal processing techniques (WT and CSS) and used them for different but related purposes: pattern recognition and shape analysis of otolith images.

The WT appears to be an efficient tool for describing otolith contours in a compact manner when they are represented by their zero crossings. These zero crossings correspond to singularities, and can be related to traditional landmarks. Moreover, since we can write a simple distance function from these representations, a database indexation or pattern recognition scheme is straightforward to design.

For the set of otoliths we used and the samples we tested, we observed in the results that although most of the otoliths found belong to the same species as the sample being searched for (even in the case of sheared data), there are otolith contours from different specimens that are very similar to the input sample. In fact, it must be taken into account that the zero crossing representation involves the whole contour, and even though singularities of different sizes are at

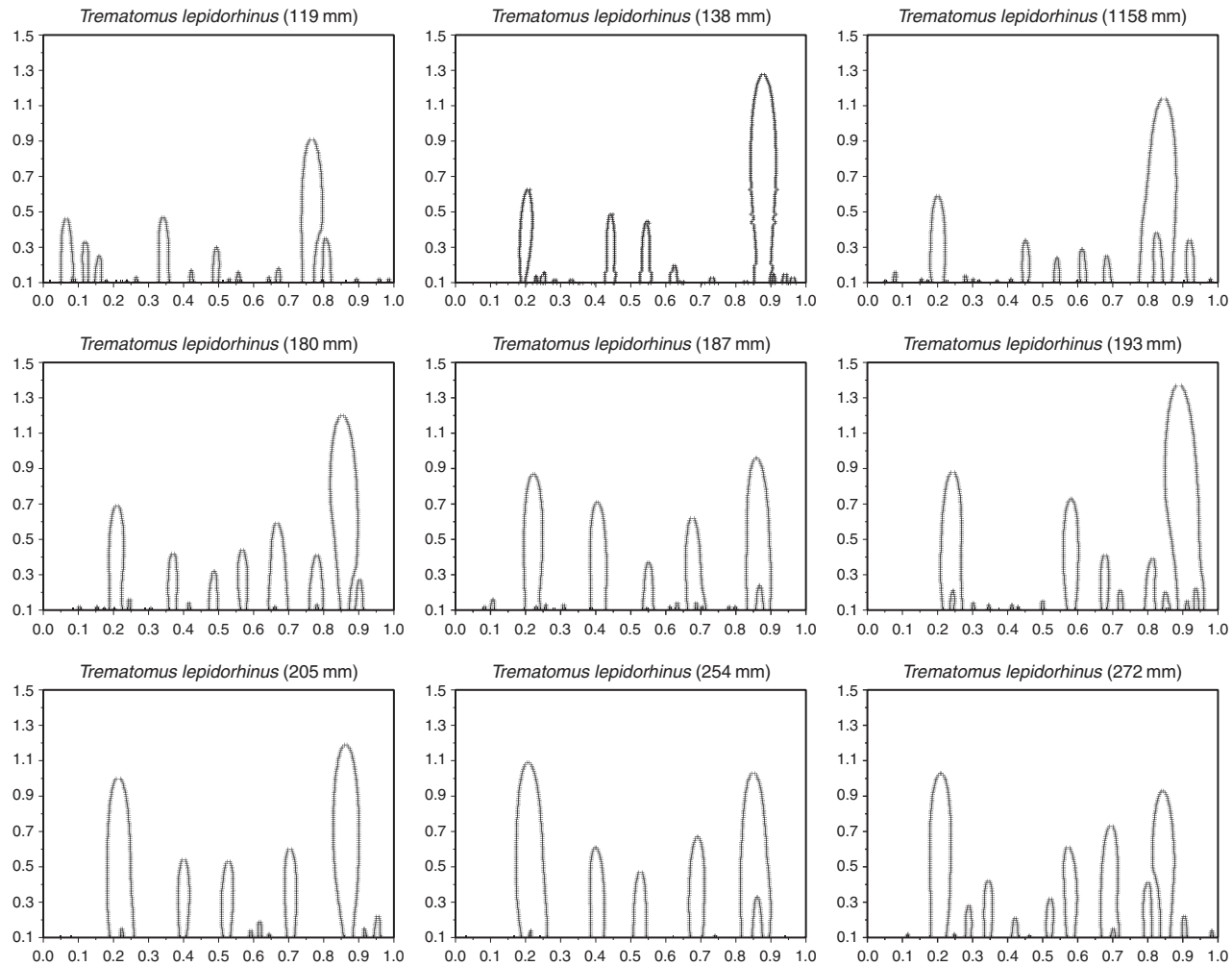

Fig. 9. Curvature scale space (CSS) otolith analysis of different sized *Trematomus lepidorhinus*.

different scales we have used all of them together. Thus, it seems that a convenient way to exploit all the properties of this kind of representation is to find the most discriminating scales and/or singularities in sets of fish otoliths, using methods which are closely related to multiresolution representations, such as Discrimination Pursuit by Buckheit and Donoho (1995) or the Local Discriminant Bases proposed by Saito and Coifman (1995).

Furthermore, using adaptive methods such as Learning Vector Quantization (Kohonen 1995) would allow us to obtain models for each set of otoliths, taking into account their class membership and providing a faster way to recognise a sample.

Additionally, one of the advantages of the zero crossings of the WT is that it reduces the amount of data needed to describe an otolith contour, which implies clear benefits for remote database retrieval through the worldwide web, this being one of the aims of the authors of this work.

The CSS shows its maximum potential when it is used as an analytical tool for mapping the curvature singularities of an otolith contour in a continuous manner. It behaves like a scale selective lens focussing on the roughness of the otolith. In the example shown in Fig. 9, it can be seen that, as the size of the fish increases there is an increase in the curvature singularities, which clearly corresponds to changes in the otolith morphology. This helps in species identification.

This increase in specific singularities in the otolith as the fish grows has been described by a morphologist (Nolf 1985) using qualitative characters and quantitative methods that do not allow these important marks to be located (Lombarte and Castellón 1991). As a consequence, using CSS is specifically directed at detecting shape changes throughout fish growth and is potentially a good tool for age identification.

Finally, we must note that both techniques, WT and CSS, have some properties in common as a result of their multiresolution and multiscale nature and provide related information about the otolith contours analysed. The WT locates the most abrupt changes at dyadic scales, while CSS maps the borders of irregular contour segments at continuous scales. It is

also possible to design a pattern recognition scheme based on CSS that is complementary to the one proposed here (Abbasi *et al*. 1999), but we chose to use the WT in this first approach because of the robustness and formalism of the distance function computed using the zero crossings of the WT.

Acknowledgments

The current work was supported by the Spanish project MICYT TIC2000–0376-p4–04. The authors wish to thank Dr Wolf Arntz for his invitation to participate in the EASIZ I and II surveys. We express our gratitude to the scientific fishing teams B. Artigues, J. González and Drs E. Balgueries, A. Schröeder and R. Knust for their help during these expeditions. The authors also acknowledge B. Morales-Nin for providing the otolith images and J. M. Marquina, R. Carrillo and A. Pintor, for their help in coding the software used in this work.

References

Abbasi, S., Mokhtarian, F., and Kittler, J. (1999). Curvature scale space image in shape similarity retrieval. *Springer Journal of MultiMedia Systems* **7**, 467–476. doi:10.1007/S005300050147

Bird, J. L., Eppler, D. T., and Checkley, D. M. (1986). Comparison of herring otoliths using Fourier series shape analyses. *Canadian Journal of Fisheries and Aquatic Sciences* **43**, 1228–1234.

Buckheit, J., and Donoho, D. (1995). Improved lineard discrimination using time-frequency dictionaries. *Proceedings of the International Society for Optical Engineering* **2569**, 540–551.

Canny, J. (1986). A computational approach to edge detection. *IEEE Transactions on Pattern Analysis and Machine Intelligence* **8**, 679–698.

Campana, S. E., and Casselman, J. M. (1993). Stock discrimination using otolith shape analysis. *Canadian Journal of Fisheries and Aquatic Sciences* **50**, 1062–1083.

Cardinale, M., Doering-Arjes, P., Kastowsky, M., and Mosegaard, H. (2004). Effects of sex, stock, and environment on the shape of known-age Atlantic cod (*Gadus morhua*) otoliths. *Canadian Journal of Fisheries and Aquatic Sciences* **61**, 158–167. doi:10.1139/F03-151

Castonguay, M., Simard, P., and Gagnon, P. (1991). Usefulness of Fourier analysis of otolith shape for Atlantic mackerel (*Scomber scombrus*) stock discrimination. *Canadian Journal of Fisheries and Aquatic Sciences* **48**, 296–302.

Courant, R., and John, F. (1989). 'Introduction to Calculus and Analysis. Vol II.' (Springer Verlag: Berlin.)

Eastman, J. T., and Clarke, A. (1998). A comparison of adaptive radiations of Antarctic fish with those of non-Antarctic fish. In 'Fishes of Antarctica: a Biological Overview'. (Eds G. di Prisco, B. Maresca and B. Tota.) pp. 3–26. (Springer-Verlag: Berlin.)

Friedland, K. D., and Reddin, D. G. (1994). Use of otolith morphology in stock discriminations of Atlantic salmon (*Salmo salar*). *Canadian Journal of Fisheries and Aquatic Sciences* **51**, 475–480.

Klingenberg, C. P., and Ekau, W. (1996). A combined morphometric and phylogenetic analysis of an ecomorphological trend: pelagization in Antarctic fishes (Perciformes: Notothenioidei). *Biological Journal of the Linnean Society* **59**, 143–177.

Kohonen, T. (1995). 'Self-Organization and Associative Memory.' (Springer-Verlag: Berlin.)

Lombarte, A., and Castellón, A. (1991). Interespecific and intraspecific otolith variability in the genus *Merluccius* as determined by image analysis. *Canadian Journal of Zoology* **69**, 2442–2449.

Mallat, S. (1989). A theory for multiresolution signal decomposition: the wavelet representation. *IEEE Transactions on Pattern Analysis and Machine Intelligence* **11**, 674–693. doi:10.1109/34.192463

Mallat, S. (1991). Zero crossings of a wavelet transform. *IEEE Transactions on Information Theory* **37**, 1019–1033. doi:10.1109/18.86995

Marr, D., and Hildreth, E. (1980). Theory of edge detection. *Proceedings of the Royal Society of London* **207**, 187–217.

Messieh, S. N., Mac Dougall, C., and Claytor, R. (1989). Separation of Atlantic herring (*Clupea harengus*) stocks in the southern Gulf of St. Lawrence using digitised otolith morphometrics and discriminant function analysis. *Canadian Technical Report of Fisheries and Aquatic Sciences* **1647**, 1–22.

Mokhtarian, F., and Mackworth, A. K. (1992). A theory of multi-scale, curvature-based shape representation for planar curves. *IEEE Transactions on Pattern Analysis and Machine Intelligence* **14**, 789–805. doi:10.1109/34.149591

Nixon, M., and Aguado, A. (2002). 'Feature Extraction and Image Processing.' (Newnes: Oxford.)

Nolf, D. (1985). Otolith piscium. In 'Handbook of Paleoichthyology. Vol 10'. (Ed. H. P. Schultze.) pp. 1–145. (Gustav Fisher Verlag: Stuttgart.)

Saito, N., and Coifman, R. (1995). Local discriminant bases and their applications. *Journal of Mathematical Imaging and Vision* **5**, 337–358. doi:10.1007/BF01250288

Torres, G. J., Lombarte, A., and Morales-Nin, B. (2000). Sagittal otolith size and shape variability to identify geographical intraspecific differences in three species of the genus *Merluccius*. *Journal of the Marine Biological Association of the UK* **80**, 333–342. doi:10.1017/S0025315499001915

Yefanov, V. N., and Khorevin, L. D. (1979). Distinguishing populations of pink salmon, *Oncorhynchus gorbuscha*, by the size of their otoliths. *Journal of Ichthyology* **19**, 142–145.

Zahn, C. T., and Roskies, R. Z. (1972). Fourier descriptors for plane closed curves. *IEEE Transactions on Computers. Institute of Electrical and Electronics Engineers* **21**, 269–281.

Manuscript received 16 July 2004; revised 8 February 2005; and accepted 7 March 2005.